

Recent results on rare kaon and hyperon decays in NA48 experiment

N. A. Molokanova^{a*}

^a *Joint Institute for Nuclear Research*

Joliot-Curie 6, 141980 Dubna, Moscow region, Russia

Abstract

Recent results from the experiments NA48/1 and NA48/2 are reported. The first measurement of direct emission and interference terms in $K^\pm \rightarrow \pi^\pm \pi^0 \gamma$ decay has been performed in the T_π^* region $0 < T_\pi^* < 80$ MeV. Analysis of the rare kaon decays $K^\pm \rightarrow \pi^\pm \gamma \gamma$, $K^\pm \rightarrow \pi^\pm e^+ e^- \gamma$, $K^\pm \rightarrow \pi^\pm e^+ e^-$ allowed precise measurements of their branching fractions and other characteristics. Measurements of radiative hyperon decays in NA48/1 experiment are presented.

1 Introduction

The series of experiments NA48 have explored many topics in the charged and neutral kaon physics. In this paper we shall discuss some of the most recent measurements produced by two stages of the experimental program: NA48/1 and NA48/2. NA48/1 experiment (2002) has been devoted mainly to the study of rare K_S decays and has produced also some results in hyperon physics. NA48/2 (2003-2004) was designed to search for direct CP-violation in K^\pm decays, but also many additional results in rare decays have been achieved.

2 Experimental setup

The NA48 detector, used in all the described results, has been designed to measure characteristics of both charged and neutral particles with high precision. The charged particle reconstruction is provided by the magnetic spectrometer with 4 drift chambers and a magnet, the momentum resolution is $\sigma_p/p = (1.02 \oplus 0.044p)\%$, where p is in GeV/ c . A charged hodoscope with a good time resolution sends the fast trigger signals representing the number of charged particles. The reconstruction of photon energy, time and position is given by a liquid krypton (LKr) calorimeter. The calorimeter has an active volume of 10 m³ with energy resolution of $\sigma(E)/E = 3.2\%/\sqrt{E} \oplus 9\%/E \oplus 0.42\%$ and space resolution of $\sigma_x = \sigma_y = 0.42/\sqrt{E} \oplus 0.06$ cm, where the energy E is in GeV. To distinguish muons from pions the hadronic calorimeter and muon counter have been used. A detailed description of NA48 beam line and detectors can be found in [1].

The measurements reported in the present paper have been obtained using different beam line configurations. The NA48 beam line was designed to produce and transport both K_L and K_S beams simultaneously. The K_L beam was produced by SPS 450 GeV/ c proton beam impinging on the beryllium target. The beginning of the decay volume was defined by the last of three collimators, located 126 m downstream of the target.

For the NA48/1 experiment the K_L beam has been removed and the proton flux on the K_S target was greatly increased. A 24 mm platinum absorber was placed after the Be target

*e-mail: Natalia.Molokanova@jinr.ru

to reduce the photon flux in the neutral beam. Using this beam line, together with the rare K_S , NA48/1 produced many hyperon decays. Investigation results of $\Xi^0 \rightarrow \Lambda\gamma$ and $\Xi^0 \rightarrow \Sigma\gamma$ decays and the first measurement of $\Xi^0 \rightarrow \Lambda e^+e^-$ will be discussed in this paper.

Since 2003 the neutral beams were replaced by simultaneous K^+ and K^- beams for the NA48/2 experiment. The momentum (60 ± 3) GeV/c was formed symmetrically for K^+ and K^- in the first achromat (fig.1), in which the two beams were split in the vertical plane. In the second achromat two of the three stations of the Kaon beam spectrometer (KABES) were placed. The beams followed the same path in the decay volume are comprised by the 114 m long cylindrical vacuum tank. The beam axes coincided to 1 mm, while their lateral size is about 1 cm.

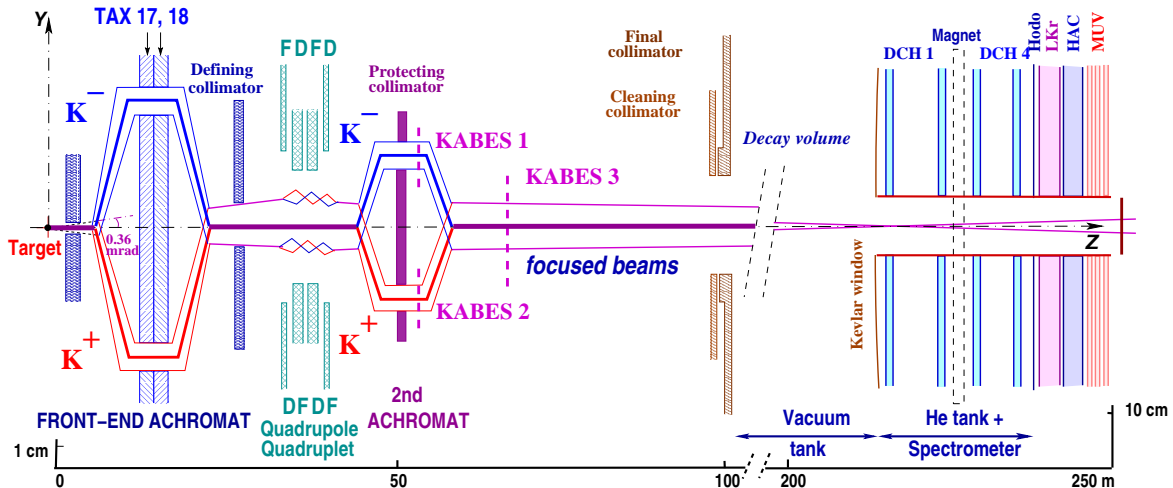


Figure 1: Schematic side view of the NA48/2 beam line (TAX 17,18: motorized beam dump/collimators used to select the momentum of the K^+ and K^- beams; FDFD/DFDF: focusing quadrupoles, KABES1–3: kaon beam spectrometer stations), decay volume and detector (DCH1–4: drift chamber, HOD: hodoscope, LKr: EM calorimeter, HAC: hadron calorimeter, MUV: muon veto). Thick lines indicate beam axes, narrow ones – the projection of their envelopes. Note that the vertical scales are different in the two parts of the figure.

3 The radiative decay $K^\pm \rightarrow \pi^\pm\pi^0\gamma$

The decay channel $K^\pm \rightarrow \pi^\pm\pi^0\gamma$ is one of the most interesting and important channels for studying the low energy structure of QCD. Three components contribute to $K^\pm \rightarrow \pi^\pm\pi^0\gamma$ decay amplitude: the Inner Bremsstrahlung (IB) that is the decay $K^\pm \rightarrow \pi^\pm\pi^0$ with a photon emitted from the outgoing charged pion, Direct Emission (DE) from the vertex and the interference (INT) between these two. The $K^\pm \rightarrow \pi^\pm\pi^0\gamma$ decays are described in terms of two kinematic variables: the kinetic energy of charged pion in kaon rest frame (T_π^*) and invariant

$$W^2 = \frac{(P_K \cdot P_\gamma)(P_\pi \cdot P_\gamma)}{(m_K m_\pi)^2},$$

where P_K , P_π , P_γ are the 4-momenta of the kaon, charged pion and odd gamma, respectively.

In fig.2a the data kaon mass spectrum is compared with the sum of $K^\pm \rightarrow \pi^\pm\pi^0\gamma$ and $K^\pm \rightarrow \pi^\pm\pi^0\pi^0$ Monte Carlo ones. The figure shows that the background contribution is very low and it can be explained in terms of $K^\pm \rightarrow \pi^\pm\pi^0\pi^0$ only.

About 124×10^3 events were selected in the range $T_\pi^* < 80$ MeV and $0.2 < W < 0.9$. In the previous measurements [2] a lower cut $T_\pi^* > 55$ MeV was introduced in order to suppress

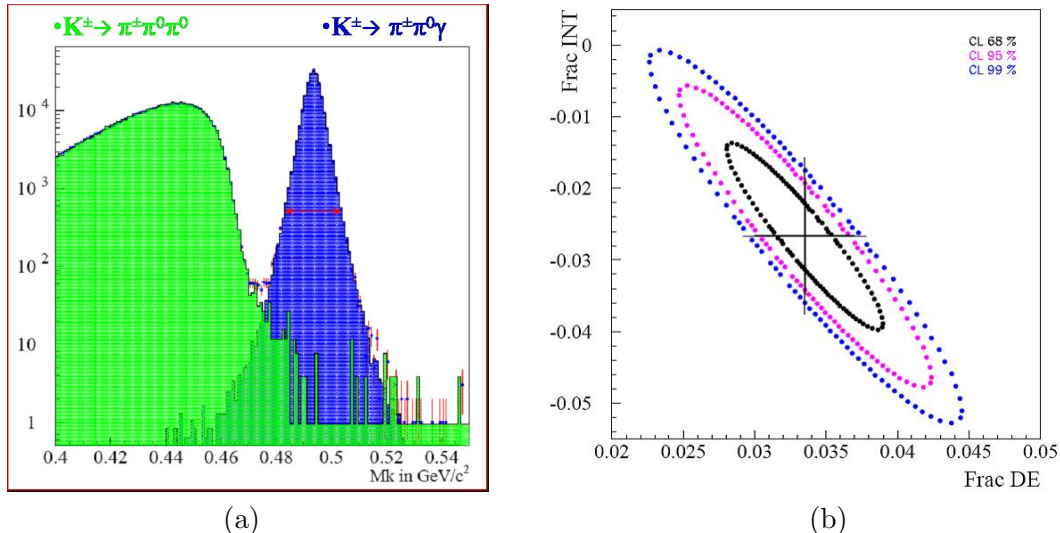


Figure 2: (a) Data–MC comparison of M_K spectrum. Dots represent data points, green distribution (left side of the histogram) – $K^\pm \rightarrow \pi^\pm\pi^0\pi^0$ MC background and the blue one (right side) the simulated signal. (b) Contour plot shows DE and INT components.

$K^\pm \rightarrow \pi^\pm\pi^0\pi^0$ and $K^\pm \rightarrow \pi^\pm\pi^0$ background. In NA48/2 measurement these backgrounds are avoided by means of the special algorithm, that detects overlapping gamma in the detector and due to the limit of ± 10 MeV on the deviation of reconstructed kaon mass from its nominal value. The upper cut on T_π^* rejects $K^\pm \rightarrow \pi^\pm\pi^0$ decays. The background in the selected sample is kept under 10^{-4} . The probability of the photon mistagging (i.e. choice of wrong odd photon) is estimated to be less than 0.1%.

The preliminary values for the fractions of DE and INT with respect to IB are

$$Frac(DE) = (3.35 \pm 0.35_{stat} \pm 0.25_{syst})\%$$

$$Frac(INT) = (-2.67 \pm 0.81_{stat} \pm 0.73_{syst})\%.$$

This is the first measurement of a non vanishing interference term in the $K^\pm \rightarrow \pi^\pm\pi^0\gamma$ decay. The contour plot in fig.2b shows the high correlation of the two distributions, correlation coefficient $\rho = -0.92$. Major improvement in the precision of measurement is expected due to the usage of the full 2003-2004 data set.

4 $K^\pm \rightarrow \pi^\pm\gamma\gamma$ analysis

The $K^\pm \rightarrow \pi^\pm\gamma\gamma$ rate is measured with respect to the $K^\pm \rightarrow \pi^\pm\pi^0$ normalization channel. The signal and normalization channels have identical particle composition of the final states, and the only cut that is different for the two channels is the one on the $\gamma\gamma$ invariant mass.

About 40% of the total NA48/2 data sample have been analyzed, and 1,164 $K^\pm \rightarrow \pi^\pm\gamma\gamma$ decay candidates (with background contamination estimated by MC to be 3.3%) are found (fig.3a). It is to be compared with the only previous experiment [3] involving 31 decay candidates. The reconstructed spectrum of $\gamma\gamma$ invariant mass in the kinematic region $M_{\gamma\gamma} > 0.2$ GeV/ c^2 is presented in fig.3b, alongside with the MC expectation assuming ChPT $\mathcal{O}(p^6)$ distribution [4] with a realistic parameter value $\hat{c} = 2$. ChPT predicts an enhancement of the decay rate (cusp-like behavior) at the $\pi\pi$ mass threshold $m_{\gamma\gamma} \sim 280$ MeV/ c^2 , independently of the \hat{c} value. The observed spectrum provides the first clean experimental evidence of this phenomenon.

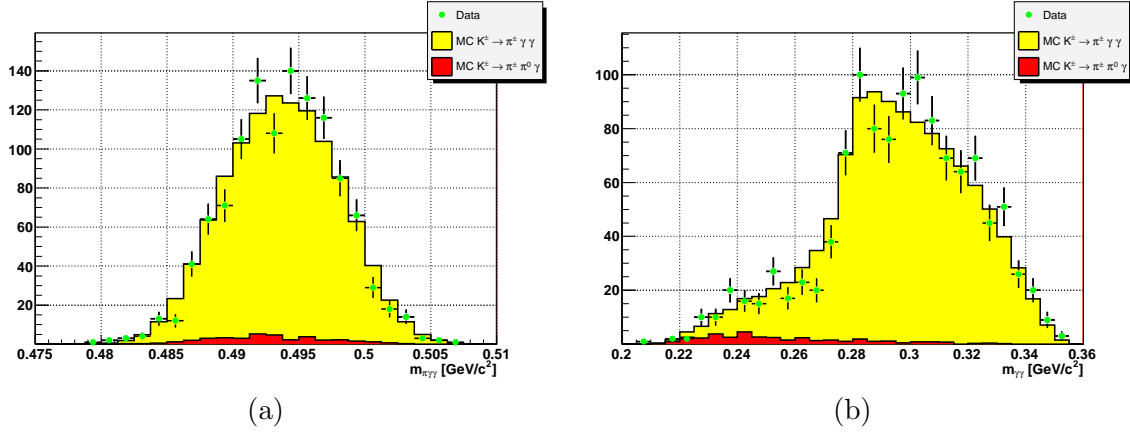


Figure 3: The reconstructed spectrum of the $\pi^\pm\gamma\gamma$ (a) and $\gamma\gamma$ (b) invariant mass for the $K^\pm \rightarrow \pi^\pm\gamma\gamma$ decay (dots), and its comparison to MC expectation assuming ChPT $\mathcal{O}(p^6)$ distribution with $\hat{c} = 2$ (filled area).

As the first step of the analysis, the partial width of the decay was measured assuming the ChPT $\mathcal{O}(p^6)$ shape with a fixed parameter $\hat{c} = 2$. The following preliminary result, which is in agreement with the ChPT computation for $\hat{c} = 2$, has been obtained:

$$BR = (1.07 \pm 0.04_{stat} \pm 0.08_{syst}) \cdot 10^{-6}.$$

A combined fit of the $m_{\gamma\gamma}$ spectrum shape and the decay rate is foreseen to measure the \hat{c} parameter.

5 First observation of the decay $K^\pm \rightarrow \pi^\pm e^+ e^- \gamma$

The decay $K^\pm \rightarrow \pi^\pm e^+ e^- \gamma$ has a kinematics, that is very similar to the corresponding $K^\pm \rightarrow \pi^\pm \gamma\gamma$. One of the photons internally converts into a pair of electrons. The branching ratio can be naively estimated using the following relation:

$$Br(K^\pm \rightarrow \pi^\pm e^+ e^- \gamma) = Br(K^\pm \rightarrow \pi^\pm \gamma\gamma) \cdot 2\alpha = 1.6 \cdot 10^{-8},$$

where α is the fine-structure constant.

NA48/2 experiment observed for the first time the radiative decay $K^\pm \rightarrow \pi^\pm e^+ e^- \gamma$. The signal is selected between 480 MeV/ c^2 and 505 MeV/ c^2 of the $\pi^\pm e^+ e^- \gamma$ invariant mass and requiring the invariant $e^+ e^- \gamma$ mass to be greater than 260 MeV/ c^2 . Fig.4 displays the projections of this region on the corresponding axes. The crosses represent data while the filled distribution represent different simulated background contribution. 120 candidates were selected with 7.3 ± 1.7 estimated background. The main source of BG is the $K^\pm \rightarrow \pi^\pm \pi_D^0 \gamma$ with a lost γ .

By using $K^\pm \rightarrow \pi^\pm \pi^0$ as a normalization channel the branching ratio was preliminary estimated to be

$$Br(K^\pm \rightarrow \pi^\pm \pi^0 \gamma) = (1.19 \pm 0.12_{stat} \pm 0.04_{syst}) \cdot 10^{-8}.$$

More details on $K^\pm \rightarrow \pi^\pm e^+ e^- \gamma$ decay analysis could be found in [5].

6 $K^\pm \rightarrow \pi^\pm e^+ e^-$ analysis

The flavour-changing neutral current process $K^\pm \rightarrow \pi^\pm e^+ e^-$, induced at one-loop level in the Standard Model and highly suppressed by the GIM mechanism, has been described by

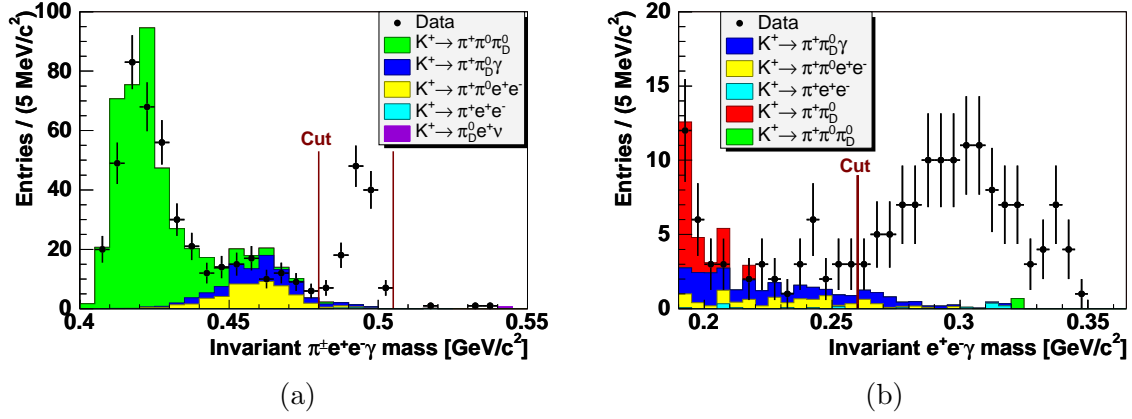


Figure 4: $K^\pm \rightarrow \pi^\pm e^+ e^- \gamma$ decay. The invariant $\pi^\pm e^+ e^- \gamma$ (a) and $e^+ e^- \gamma$ (b) masses with corresponding background distributions. Black crosses represent data distribution.

ChPT [6]. Several models predicting the form factor characterizing the dilepton invariant mass spectrum and the decay rate have been proposed [7, 8]. The decay was first studied at CERN [9], then this study has been followed by BNL E777 [10] and E865 [11] measurements.

Signal and normalization samples. The $K^\pm \rightarrow \pi^\pm e^+ e^-$ rate is measured with respect to the abundant $K^\pm \rightarrow \pi^\pm \pi_D^0$ normalization channel (with $\pi_D^0 \rightarrow e^+ e^- \gamma$). The final states of the signal and normalization channels contain identical sets of charged particles. Thus electron and pion identification efficiencies, potentially representing a significant source of systematic uncertainties, cancel in the first order.

The reconstructed $\pi^\pm e^+ e^-$ invariant mass spectrum is presented in fig.5a. The $\pi^\pm e^+ e^-$ mass resolution is $\sigma_{\pi ee} = 4.2 \text{ MeV}/c^2$, in agreement with MC simulation.

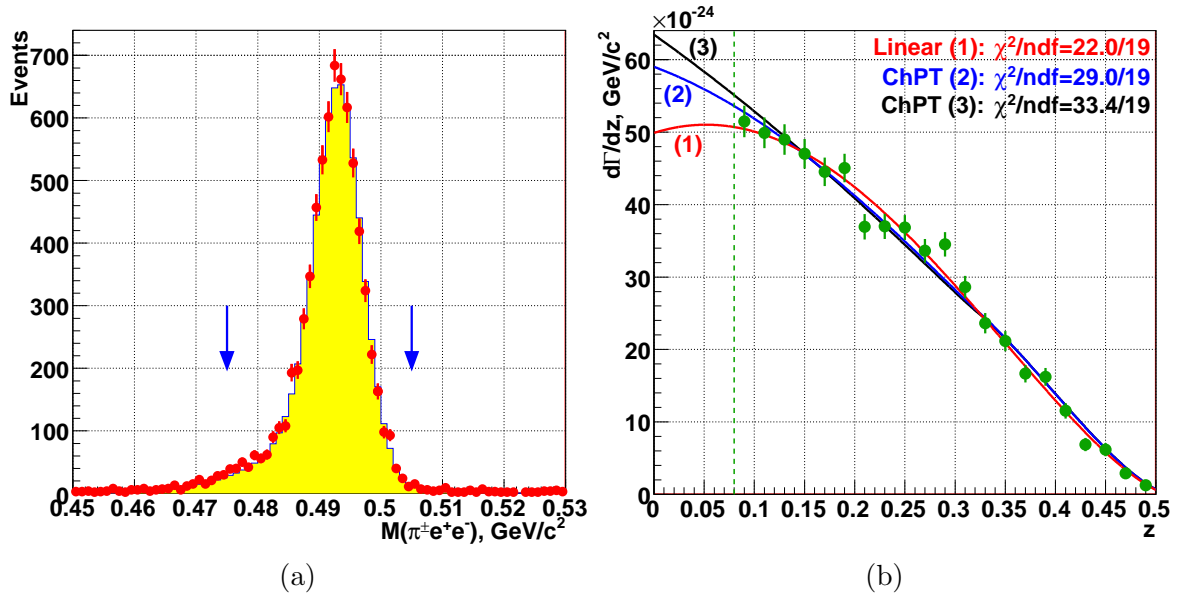


Figure 5: (a) Reconstructed spectrum of $\pi^\pm e^+ e^-$ invariant mass; data (dots) and MC simulation (filled area). (b) The computed $d\Gamma_{\pi ee}/dz$ (background subtracted) and the results of fits according to the considered models (see description in text).

In total 7,146 $K^\pm \rightarrow \pi^\pm e^+ e^-$ candidates have been found in the signal region. After the

kinematical suppression of the π_D^0 decays, residual background contamination mostly results from particle misidentification (i.e. e^\pm identified as π^\pm and vice versa). The following relevant background sources were investigated with MC simulations: $K^\pm \rightarrow \pi^\pm \pi_D^0$ with misidentified e^\pm and π^\pm ; $K^\pm \rightarrow \pi_D^0 e^\pm \nu$ with a misidentified e^\pm from the π_D^0 decay. Background estimation by selecting of the strongly suppressed [12] lepton number violating $K^\mp \rightarrow \pi^\mp e^\pm e^\pm$ ("same-sign") candidates is considered to be the most reliable method. For the above two background sources, the expected mean numbers and kinematic distributions of the selected same-sign candidates are identical to those of background events (up to the negligible acceptance correction). In total 44 events pass the same-sign selection, which leads to the background estimation of $(0.6 \pm 0.1)\%$. This result is independently confirmed by MC simulation of the two background modes.

In total $12,228 \times 10^6$ $K^\pm \rightarrow \pi^\pm \pi_D^0$ candidates were found in the signal region. The only significant background source is the semileptonic $K^\pm \rightarrow \pi_D^0 \mu^\pm \nu$ decay. Its contribution is not suppressed by particle identification cuts, since no π/μ separation is performed. The background contamination is estimated by MC simulation to be 0.15%.

Theoretical input. The decay is supposed to proceed through one-photon exchange, resulting in a spectrum of the $z = (M_{ee}/M_K)^2$ kinematic variable, sensitive to the form factor $W(z)$ [7]

$$\frac{d\Gamma}{dz} = \frac{\alpha^2 M_K}{12\pi(4\pi)^4} \lambda^{3/2}(1, z, r_\pi^2) \sqrt{1 - 4\frac{r_e^2}{z}} \left(1 + 2\frac{r_e^2}{z}\right) |W(z)|^2,$$

where $r_e = m_e/M_K$, $r_\pi = m_\pi/M_K$, and $\lambda(a, b, c) = a^2 + b^2 + c^2 - 2ab - 2ac - 2bc$. On the other hand, the spectrum of the angle $\theta_{\pi e}$ between π and e^+ in the e^+e^- rest frame is proportional to $\sin^2(\theta_{\pi e})$, and is not sensitive to $W(z)$.

The following parameterizations of the form factor $W(z)$ are considered in the present analysis:

1. Linear: $W(z) = G_F M_K^2 f_0(1 + \delta z)$ with free normalization and slope (f_0, δ).
2. Next-to-leading order ChPT [7]: $W(z) = G_F M_K^2 (a_+ + b_+ z) + W^{\pi\pi}(z)$ with free parameters (a_+, b_+), and an explicitly calculated pion loop term $W^{\pi\pi}(z)$.
3. ChPT parameterization involving meson form factors: $W(z) \equiv W(M_a, M_\rho, z)$ [8], with resonance masses (M_a, M_ρ) treated as free parameters.

The analysis goal is the extraction of the form factor parameters in the framework of each of the above models, and computation of the corresponding branching fractions $BR_{1,2,3}$.

The computed values of $d\Gamma_{\pi ee}/dz$ vs z are presented in fig.5b alongside with the results of the fits to three considered models. $BR(K^\pm \rightarrow \pi^\pm e^+ e^-)$ in the full kinematic range corresponding to each model are then computed using the measured parameters, their statistical uncertainties, and correlation matrices.

In addition, a model-independent branching fraction $BR(z > 0.08)$ in the visible kinematic region $z > 0.08$ is computed by integration of $d\Gamma_{\pi ee}/dz$. $BR(z > 0.08)$ is to a good approximation equal to each of the model-dependent BR s computed in the restricted kinematic range $z > 0.08$.

Results. Fits to all the three models are of reasonable quality, however the linear form-factor model leads to the smallest χ^2 . The data sample is insufficient to choose the best of the models considered.

The branching ratio in the full kinematic range, which is computed as the average between the two extreme cases corresponding to the models (1) and (3), and includes an uncertainty due to extrapolation into the region $z < 0.08$, is

$$BR = (3.08 \pm 0.04_{stat} \pm 0.04_{syst} \pm 0.08_{ext} \pm 0.07_{model}) \cdot 10^{-7} = (3.08 \pm 0.12) \cdot 10^{-7}.$$

It should be stressed that a large fraction of the uncertainty of this result is correlated with the earlier measurements. A comparison to the precise BNL E865 measurement [13] dismissing correlated uncertainties due to external BR s and model dependence, and using the same external input, shows a 1.4σ difference. In conclusion, the obtained BR is in agreement with the previous measurements.

Finally, a first measurement of the direct CP violating asymmetry of K^+ and K^- decay rates in the full kinematic range was obtained by performing BR measurements separately for K^+ and K^- and neglecting the correlated uncertainties:

$$\Delta(K_{\pi ee}^{\pm}) = (BR^+ - BR^-)/(BR^+ + BR^-) = (-2.1 \pm 1.5_{stat} \pm 0.3_{syst})\%.$$

The result is compatible with the absence of CP violation. However its precision is far from the theoretical expectation [7] of $|\Delta(K_{\pi ee}^{\pm})| \sim 10^{-5}$.

More details on the event selection, trigger efficiency, fitting procedure, analysis of systematics could be found in [14].

7 Weak radiative Ξ^0 decays

Up to this day weak radiative hyperon decays as $\Xi^0 \rightarrow \Lambda\gamma$ and $\Xi^0 \rightarrow \Sigma\gamma$ are barely understood. Several theoretical models exist, which give very different predictions. A usual experimental parameter to distinguish between models is the decay asymmetry α . It is defined by

$$\frac{dN}{d\cos(\theta)} = N_0 (1 + \alpha \cos(\theta)),$$

where θ is the angle between the direction of the daughter baryon flight and the polarization of Ξ^0 in its rest frame. In particular, the decay asymmetry for $\Xi^0 \rightarrow \Lambda\gamma$ can be measured by looking at the angle between the incoming Ξ and the outgoing proton from the subsequent $\Lambda \rightarrow p\pi^-$ decay in the Λ rest frame (fig.6). Using this method, the measurement is independent of the unknown initial Ξ^0 polarization.

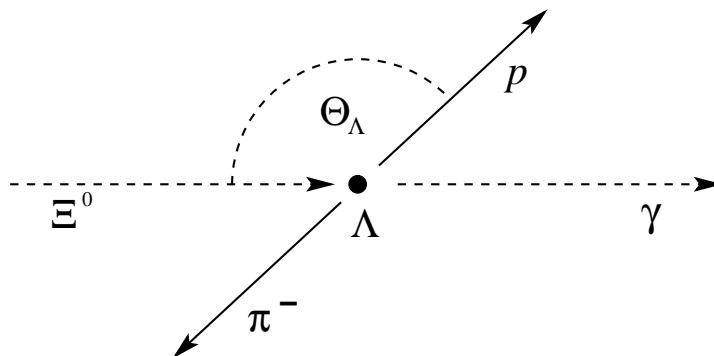


Figure 6: Definition of the angle θ between the proton and the incoming Ξ^0 in the Λ rest frame.

The NA48/1 experiment has selected 48,314 $\Xi^0 \rightarrow \Lambda\gamma$ and 13,068 $\Xi^0 \rightarrow \Sigma\gamma$ candidates (fig.7). The background contributions are 0.8% for $\Xi^0 \rightarrow \Lambda\gamma$ and about 3% for $\Xi^0 \rightarrow \Sigma\gamma$, respectively.

Using these data, fits to the decay asymmetries have been performed. In case of $\Xi^0 \rightarrow \Sigma\gamma$, where we have the subsequent decay $\Sigma^0 \rightarrow \Lambda\gamma$, the product $\cos(\theta_{\Xi \rightarrow \Sigma\gamma}) \cdot \cos(\theta_{\Sigma \rightarrow \Lambda\gamma})$ has to be used for the fit. Both fits show the expected linear behavior on the angular parameters (fig.8).

After correcting for the well-known asymmetry of $\Lambda \rightarrow p\pi^-$, values of

$$\alpha_{\Xi^0 \rightarrow \Lambda\gamma} = -0.684 \pm 0.020_{stat} \pm 0.061_{syst}$$

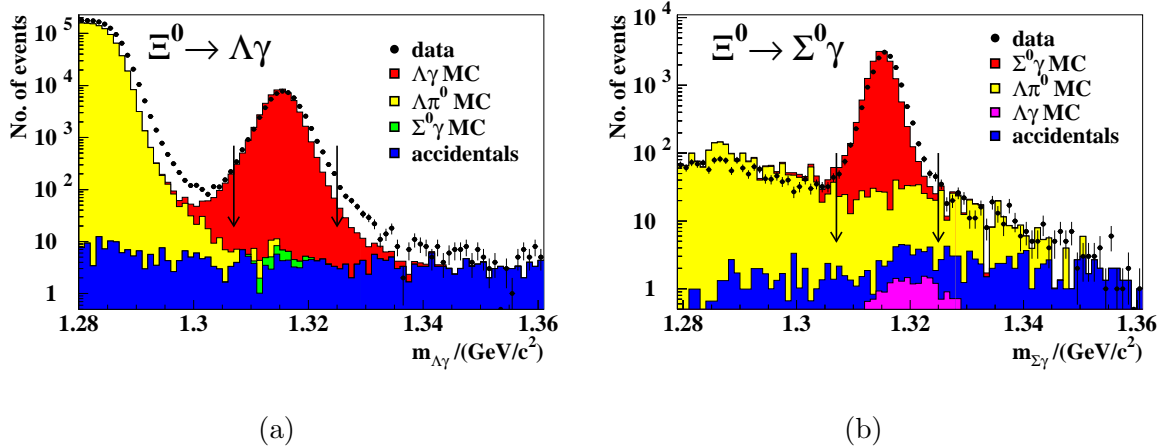


Figure 7: $\Xi^0 \rightarrow \Lambda\gamma$ (a) and $\Xi^0 \rightarrow \Sigma\gamma$ (b) signal together with MC expectations for signals and backgrounds.

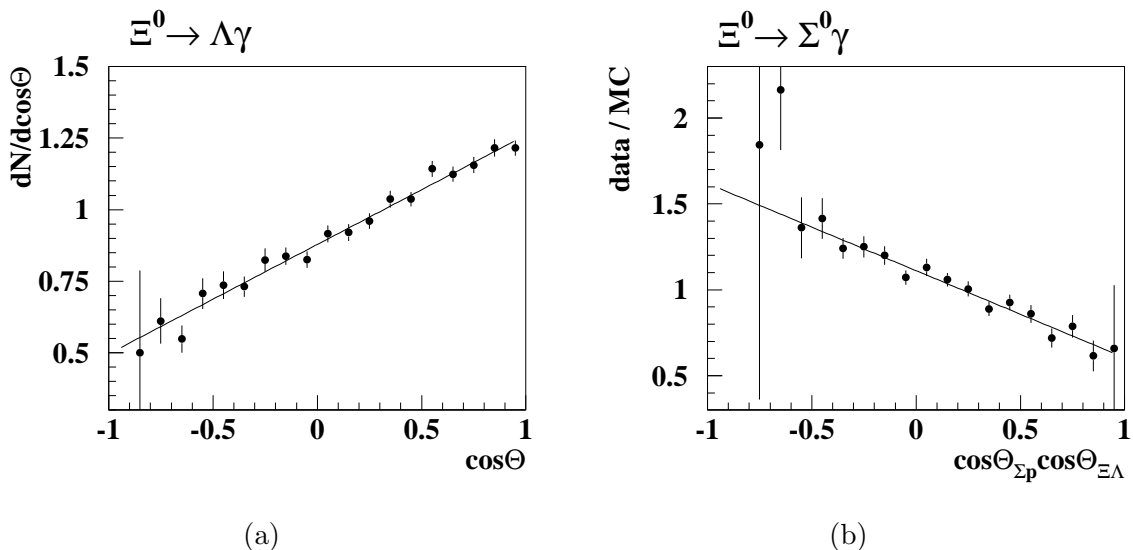


Figure 8: Fits of the decay asymmetries in $\Xi^0 \rightarrow \Lambda\gamma$ (a) and $\Xi^0 \rightarrow \Sigma\gamma$ (b).

and

$$\alpha_{\Xi^0 \rightarrow \Sigma\gamma} = -0.682 \pm 0.031_{stat} \pm 0.065_{syst}$$

are obtained. These values agree with previous measurements by NA48 on $\Xi^0 \rightarrow \Lambda\gamma$ [15] and KTeV on $\Xi^0 \rightarrow \Sigma\gamma$ [16], but are much more precise. In particular the result on $\Xi^0 \rightarrow \Lambda\gamma$ is of high theoretical interest, as it confirms the large negative value of the decay asymmetry, which is difficult to accommodate in the frameworks of the quark and vector meson dominance models.

8 First observation of $\Xi^0 \rightarrow \Lambda e^+ e^-$

In the 2002 run of NA48/1 experiment the weak radiative decay $\Xi^0 \rightarrow \Lambda e^+ e^-$ has been detected for the first time. 412 candidates were selected with 15 background events (fig.9) The

obtained branching fraction

$$Br(\Xi^0 \rightarrow \Lambda e^+ e^-) = (7.6 \pm 0.4_{stat} \pm 0.4_{syst} \pm 0.2_{norm}) \cdot 10^{-6}$$

is consistent with inner bremsstrahlung-like e^+e^- production mechanism.

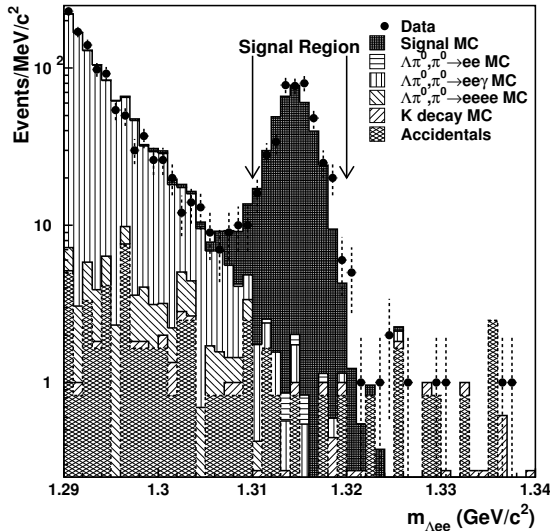


Figure 9: The invariant mass of $\Lambda e^+ e^-$ together with the simulated background.

The decay parameter $\alpha_{\Xi\Lambda ee}$ can be measured from the angular distribution

$$\frac{dN}{d\cos(\theta_{p\Xi})} = \frac{N}{2} (1 - \alpha_{\Xi\Lambda ee} \alpha_- \cos(\theta_{p\Xi})), \quad (1)$$

where $\cos(\theta_{p\Xi})$ is the angle between the proton from $\Lambda \rightarrow p\pi$ decay relative to the Ξ^0 line of flight in the Λ rest frame and α_- is the asymmetry parameter for the decay $\Lambda \rightarrow p\pi^-$. The obtained value

$$\alpha_{\Xi\Lambda ee} = -0.8 \pm 0.2$$

is consistent with the latest published value of the decay asymmetry parameter for $\Xi \rightarrow \Lambda\gamma$. Details on the analysis can be found in [17].

9 Conclusion

The first measurement of direct emission and interference contributions to the decay $K^\pm \rightarrow \pi^\pm \pi^0 \gamma$ with a non-zero interference term has been obtained, uncertainty is dominated by statistical error.

A precise study of the $K^\pm \rightarrow \pi^\pm \gamma \gamma$ has been performed. The first clear evidence for a rate enhancement at $\pi\pi$ mass threshold has been obtained. The preliminary measurement of BR agrees with the ChPT prediction. A detailed spectrum shape study is foreseen.

The first observation and measurement of parameters of the $K^\pm \rightarrow \pi^\pm e^+ e^- \gamma$ decay, including the BR , have been performed. The $M_{ee\gamma}$ spectrum provides an evidence for the cusp at the $\pi\pi$ mass threshold.

A precise study of the $K^\pm \rightarrow \pi^\pm e^+ e^-$ decay has been performed. The data sample and precision are compatible to the world best ones. The preliminary results are in agreement with the previous measurements. The first limit on CP violating charge asymmetry has been obtained.

In NA48/1 radiative hyperon decays $\Xi^0 \rightarrow \Lambda\gamma$ and $\Xi^0 \rightarrow \Sigma\gamma$ have been investigated, measurements of BR and decay asymmetries α of these decays have been performed. $\Xi^0 \rightarrow \Lambda e^+ e^-$ decay has been observed for the first time. BR and decay parameter α have been measured as well.

References

- [1] V.Fanti et al., *Nucl.Instrum.Meth.* **A** 574, 433 (2007).
A.Lai et al., *Eur.Phys.J.* **C** 22, 231 (2001).
J.R.Batley et al., *Phys.Lett.* **B** 544, 97 (2002).
- [2] R.J.Abrams et al., *Phys.Rev.Lett.* **29**, 1118 (1972).
S.C.Adler et al., *Phys.Rev.Lett.* **85**, 4856 (2000).
M.A.Aliev et al., *Phys.Lett.* **B** 554, 7 (2003).
M.A.Aliev et al., *Eur.Phys.J.* **C** 46, 61 (2006).
- [3] P.Kitching et al., *Phys.Rev.Lett.* **79**, 4079 (1997).
- [4] G.D'Ambrosio, J.Portolés, *Phys.Lett.* **B** 386, 403 (1996).
- [5] J.R.Batley et al., *Phys.Lett.* **B** 659, 493 (2008).
- [6] G.Ecker, A.Pich, E.de Rafael, *Nucl.Phys.* **B** 291, 692 (1987).
- [7] G. D'Ambrosio et al., *JHEP* **8**, 4 (1998).
- [8] A.Z.Dubničková et al., *Phys.Part.Nucl.Lett.* **5**, vol. 2, 76 (2008) [hep-ph/0611175].
- [9] P.Bloch et al., *Phys.Lett.* **B** 56, 201 (1975).
- [10] C.Alliegro et al., *Phys.Rev.Lett.* **68**, 278 (1992).
- [11] R.Appel et al., *Phys.Rev.Lett.* **83**, 4482 (1999).
- [12] R.Appel et al., *Phys.Rev.Lett.* **85**, 2877 (2000).
- [13] R.Appel et al., *Phys.Rev.Lett.* **83**, 4482 (1999).
- [14] E.Goudzovski, arXiv:0803.4475.
- [15] A.Lai et al, *Phys.Lett.* **B** 584, 251 (2004).
- [16] A.Alavi-Harati et al, *Phys.Rev.Lett.* **86**, 3239 (2001).
- [17] J.R.Batley et al, *Phys.Lett.* **B** 650, 1 (2007).